INORGANIC CHEMISTRY FRONTIERS

RESEARCH ARTICLE

View Article Online
View Journal | View Issue

Cite this: *Inorg. Chem. Front.*, 2024, **11**, 7853

Modulating the birefringence of two-dimensional hybrid lead bromide perovskites using pyridine derivative cations†

Li-Ling Zhang,‡ Hua Huang,‡ Qingran Ding, Hui-Ping Xiao, Qing-Yan Liu * and Yu-Ling Wang *

Received 19th June 2024,
Accepted 8th October 2024

DOI: 10.1039/d4qi01547a

rsc.li/frontiers-inorganic

Birefringent crystals for modulating the polarization of light are of technological importance in optical communications. Herein we provide two novel two-dimensional hybrid halide perovskites, [(H_2-dpys)($PbBr_4$)] (**1**) (dpys = di(pyridin-4-yl)sulfane) and [(H-cmpy)$_4$(Pb_3Br_{10})] (**2**) (cmpy = 4-chloro-3-methylpyridine), which can act as birefringent crystals. Remarkably, the crystal structures and the optoelectronic performance of the hybrid lead bromide perovskites are elaborately regulated by the organic cations of pyridine derivatives. Compound **2** constructed from the H-cmpy$^+$ cations containing the single pyridyl moiety has a significantly enhanced birefringence (0.315@550 nm) compared to compound **1** (0.192@550 nm) with two pyridyl moieties of H_2-dpys^{2+} cations, and it is larger than those of all commercial birefringent crystals and most of the hybrid metal halide perovskites. The results of the theoretical calculations showed that the highly distorted $PbBr_6$ octahedra and the delocalized π-conjugation of H-cmpy$^+$ cations synergistically contribute to the enhanced birefringence of **2**. This work provides a useful strategy for modulating the crystal structure and optoelectronic performance of the hybrid lead halide perovskites.

Introduction

Birefringent crystals show great applications in optical devices such as polarizing microscopes, polarization beam splitters, optical isolators, achromatic quarter-wave plates, and advanced optical instruments.[1–5] As a key component of the optical devices, it is desirable that the birefringent crystals have a large birefringence (Δn), which is conducive to miniaturizing polarization devices.[6] The currently used commercial birefringent crystals mainly refer to calcite with a birefringence of 0.172 at 532 nm,[7] yttrium vanadate with a birefringence of 0.204 at 532 nm,[8] titanium dioxide with a birefringence of 0.256 at 546 nm,[9] lithium niobate with a birefringence of 0.074 at 546 nm,[10] and barium metaborate with a birefringence of 0.122 at 546 nm.[11] It is known that the growth of the single crystals of the artificial birefringent crystals such as lithium niobate, yttrium vanadate, and barium metaborate is energy-intensive. Furthermore, for the natural birefringent crystals such as calcite and titanium dioxide, defects and impurities are commonly observed. Most importantly, the currently commercial birefringent crystals such as barium metaborate and magnesium fluoride have a restrictedly working wavelength and fairly small birefringence.[12,13] With the rapid development of scientific and industrial communities, the discovery of new birefringent crystals is thus of crucial scientific and technological importance.

To improve the birefringence, a general approach is to introduce different components to modulate the optical anisotropy of a crystal. It is known that the planar π-conjugated groups generally have large polarizability anisotropy, which generates large optical anisotropy to induce large birefringence.[14,15] The inorganic units with π-conjugated structures such as BO_3,[16,17] CO_3,[18] and NO_3 [19] units are the extensively explored birefringent functional active groups. Recently, organic groups with a planar structure, which act as birefringent functional units, have been utilized for the construction of birefringent crystals.[20–22] Besides, metal cations possessing stereochemical activity lone pairs such as Pb^{2+}, Bi^{3+}, Nb^{5+}, and V^{5+} are other kinds of important birefringent functional units.[23,24] These metal cations exhibiting uneven electron distribution are particularly prone to form highly distorted polyhedra, resulting in large birefringence. With these in mind, the π-conjugated pyridine molecules and Pb^{2+} with a lone pair

College of Chemistry and Materials, Key Lab of Fluorine and Silicon for Energy Materials and Chemistry of Ministry of Education and National Engineering Research Centre for Carbohydrate Synthesis, Jiangxi Normal University, Nanchang 330022, China. E-mail: qyliuchem@jxnu.edu.cn, ylwang@jxnu.edu.cn

†Electronic supplementary information (ESI) available. CCDC 2361167 and 2361168. For ESI and crystallographic data in CIF or other electronic format see DOI: https://doi.org/10.1039/d4qi01547a

‡These authors contributed equally to this work.

were utilized for constructing birefringent crystals. Two novel birefringent crystals, namely, $[(H_2\text{-dpys})(PbBr_4)]$ (**1**) (dpys = di(pyridin-4-yl)sulfane) and $[(H\text{-cmpy})_4(Pb_3Br_{10})]$ (**2**) (cmpy = 4-chloro-3-methylpyridine), were obtained from similar reactions. Compounds **1** and **2** are two-dimensional (2-D) hybrid halide perovskites exhibiting different structures and optoelectronic performances. It is interesting that the crystal structures and optoelectronic performance of the present hybrid lead halide perovskites are modulated by the pyridine derivative cations. Compound **2** with large polarization anisotropy displays a large birefringence of 0.315 at 550 nm, and outperforms all commercial birefringent crystals and almost all reported hybrid halide perovskites. The microscopic mechanism of the optical properties of these materials is disclosed through theoretical calculations.

Results and discussion

The optical photographs of crystals **1** and **2** are provided in Fig. 1. In the presence of different organic pyridine molecules, different 2-D lead bromide perovskites were generated. Compound **1** is crystallized in an orthogonal space group of *Pbcm* (Table S1 in ESI†). Half of a di(pyridin-4-yl)sulfane (H_2-$dpys^{2+}$) cation, half of a Pb^{2+} atom, two Br^- atoms with an occupation of 0.5, and one fully occupied Br^- atom in the asymmetric unit of **1**. The Pb^{2+} atom is coordinated with six Br^- atoms to give an octahedral coordination geometry (Fig. 1a). The Pb–Br bond lengths are between 2.9667(7) and 3.0626(9) Å (Table S2 in ESI†). The Br3 atom is a terminal ligand, whereas Br1 and Br2 atoms serve as bridging ligands. The single Pb^{2+} atoms are linked by the bridging bromide ligands to form a 2-D layer running along the *ab* plane (Fig. 2a). The anionic 2-D layer is charge-balanced by the diprotonated H_2-$dpys^{2+}$ cations, which fill the interlayered spaces (Fig. 2b) and interact with the 2-D layers through N–H···Br hydrogen bonds with a N···Br separation of 3.547(6) Å. Under a similar reaction, di((pyridin-4-yl)sulfane) was displaced with 4-chloro-3-methylpyridine, leading to compound **2**. The asymmetric unit of **2** contains one and a half Pb^{2+} atoms, five Br^- atoms, and two H-$cmpy^+$ cations. Both Pb^{2+} atoms are coordinated by six Br^- atoms in the distorted octahedral coordinated geometry (Fig. 1b) with Pb–Br bond lengths ranging from 2.9396(14) to 3.1050(14) Å (Table S2†). It is interesting that a trinuclear Pb_3Br_{12} basic unit is formed from two Pb1 atoms and a Pb2 atom bridged by six Br^- atoms (Fig. 1b). The Pb2 atom occupies an inversion center, resulting in a centrosymmetric Pb_3Br_{12} unit. Each Pb_3Br_{12} unit shares four bridging Br^- atoms with four neighboring Pb_3Br_{12} units to generate a 2-D layer propagating along the *bc* plane (Fig. 2c). The polyanionic 2-D layers in compound **2** are charge-balanced by plenty of H-$cmpy^+$ cations, which fill the interlayered spaces (Fig. 2d). The H-$cmpy^+$ cations form N–H···Br hydrogen bonds (N···Br distances of 3.270(11) and 3.482(12) Å) with the 2-D layers (Table S2†). Thus distinct 2-D lead bromide layers are constructed with different pyridine cations. Obviously, the above findings show that the structures of the 2-D lead bromide layers can be modulated by the organic cations, which provides a feasible approach for rational regulation of the structures of the hybrid metal halide perovskites.

The phase purity of both compounds was verified using powder X-ray diffraction patterns (Fig. S1†). Both compounds show high thermal stability with the temperature at the first weight loss being higher than 200 °C (Fig. S2†). Furthermore, the two compounds show high water- and humidity-resistance (Fig. S1†). The ultraviolet-visible-near-infrared diffuse reflectance spectra for compounds **1** and **2** were collected under ambient conditions with wavelengths ranging from 200 nm to 800 nm (Fig. S3†). The results of the absorption spectra give the experimental band gaps of 2.62 and 2.73 eV for **1** and **2**, respectively. The birefringence for both compounds was measured based on the transparent crystals under a cross-polarizing microscope equipped with a quartz wedge compensator. The original interference color of first-order violet was observed for crystal **1** under a cross-polarizing light (Fig. 3a). Such a color can show complete extinction as the quartz wedge compensator is rotated (Fig. 3b). The thickness for crystal **1** obtained from the polarizing microscope is 8.6 μm (Fig. 3c). With the formula of $\Delta n = R/d$, the birefringence for crystal **1** is 0.192 at 550 nm, which is much larger than those of LiB_3O_5 (0.040@532 nm)[25] and $CsLiB_6O_{10}$ (0.049@500 nm).[26] A third-order yellow-green interference color was observed for crystal **2** under orthogonally polarized light (Fig. 3d). Complete extinction was realized for crystal **2** when the compensator was rotated (Fig. 3e). The crystal thickness measured with the polarizing microscope for crystal **2** is 4.57 μm (Fig. 3e). Thus a

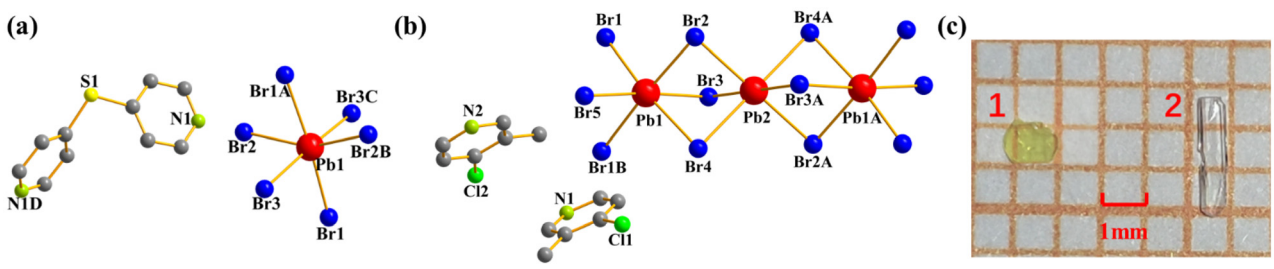

Fig. 1 (a) Crystal structures of **1** and (b) **2** showing the coordination environments of Pb^{2+} atoms (H atoms are omitted for clarity). (c) Optical photographs of crystals **1** and **2**.

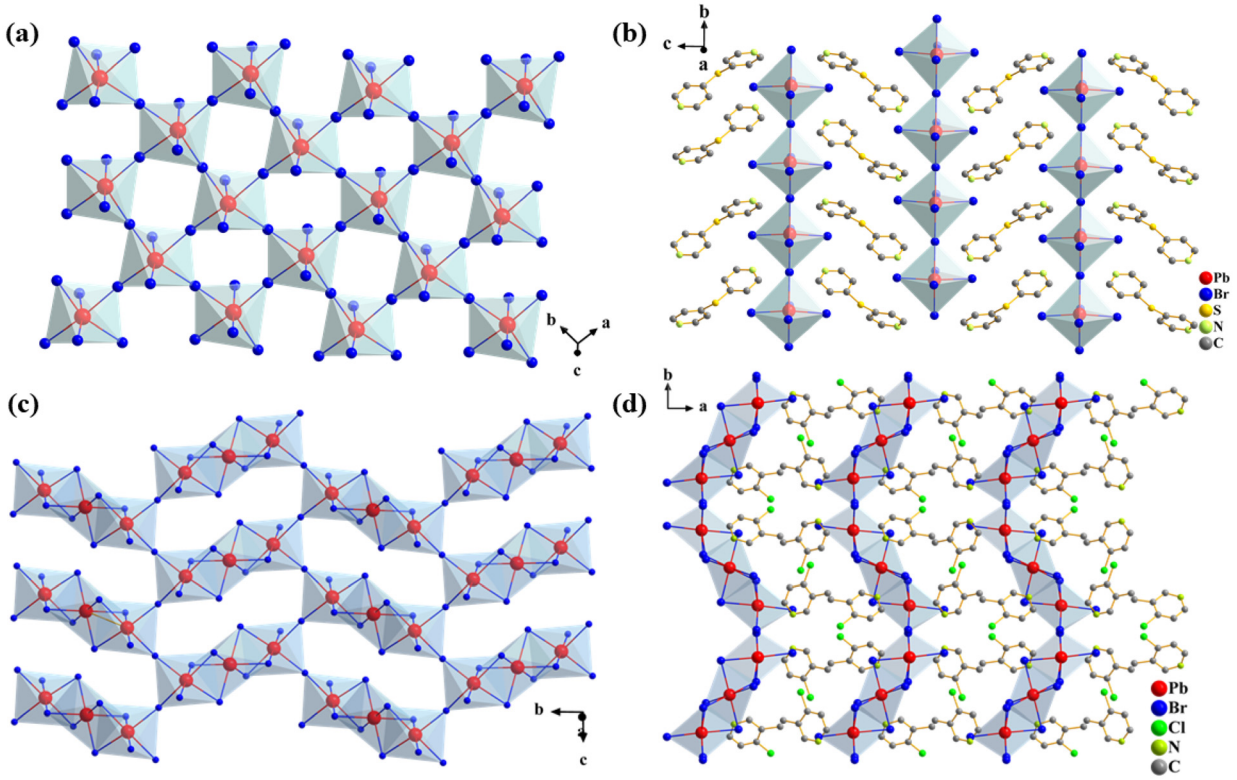

Fig. 2 (a) 2-D inorganic $[PbBr_4]_n^{2n-}$ layered structure and (b) 3-D packing structure in **1**. (c) 2-D inorganic $[Pb_3Br_{10}]_n^{4n-}$ layered structure and (d) 3-D packing structure in **2**.

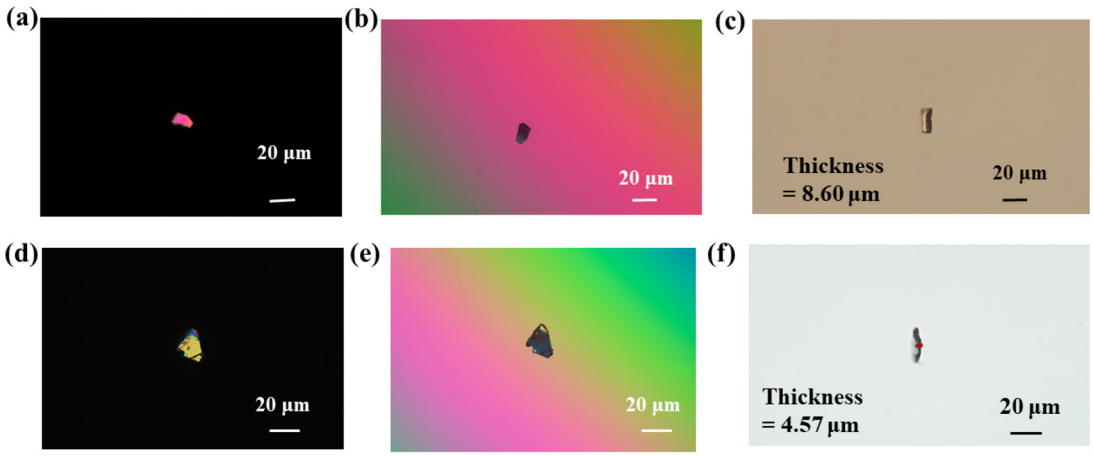

Fig. 3 Measurements of birefringence. Original interference colors for crystals **1** (a) and **2** (d). Crystals **1** (b) and **2** (e) under complete extinction. Thickness of selected crystals **1** (c) and **2** (f).

birefringence of 0.315 for **2** was obtained at 550 nm. Such large birefringence for crystal **2** is remarkable and comparable to that of the benchmark halide perovskite material $MLAPbBr_4$ (exp. 0.322@550 nm),[20] ranking it among the halide perovskite materials including $CsPbBr_3$ (cal. 0.26@550 nm),[21] LiCl ($H_3C_3N_3O_3$) (0.266@1064 nm),[27] $(C_{10}H_{11}N_3)PbBr_4$ (0.127@550 nm),[28] and $CH_3NH_3PbI_3$ (cal. 0.292@1064 nm)[29] (Fig. 4). In addition, the birefringence for crystal **2** surpasses those of all commercial birefringent crystals ($CaCO_3$ (exp. 0.172@532 nm),[7] YVO_4 (exp. 0.204@532 nm),[8] TiO_2 (exp. 0.256@546 nm) and MgF_2 (exp. 0.012@1046 nm)),[13] and other leading birefringent crystals such as $SbTeO_3Br$ (0.281@546 nm)[30] and $NaVSeO_5$ (0.180@546 nm),[31] making it a promising candidate for birefringent crystals.

For exploration of the birefringence observed for **1** and **2**, the calculated birefringence values were obtained using the

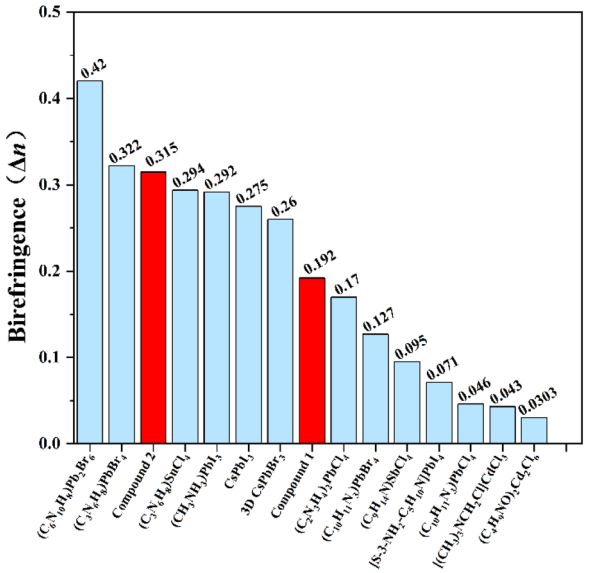

Fig. 4 Comparison of the birefringence of the hybrid metal halide perovskites.

first-principles methods. The calculation results give the theoretical values of birefringence of 0.221 for **1** and 0.296 for **2** at 550 nm (Fig. 5a and b), which are basically in line with the experimental ones. The band structures for **1** and **2** calculated using density functional theory methods are shown in Fig. S4.† The direct band gaps for **1** and **2** are 2.38 and 2.43 eV derived from the calculated results, which are consistent with the experimental findings.

The partial density of states (PDOS) and total density of states (DOS) are further provided (Fig. 5c and d). For compound **1**, the Br-4p, S-3p and Pb-6p orbitals largely contribute to the valence bands (VBs) near the Fermi level. Small amounts of C-2p and N-2p orbitals are also observed in the VBs (Fig. 5c). The bottom of conduction bands (CBs) for compound **1** are mainly composed of C-2p, N-2p, S-3p and Pb-6p orbitals. For compound **2**, the VBs near the Fermi level mainly consist of Br-4p, C-2p, Pb-6p, and Cl-3p orbitals hybridized with a small amount of N-2p orbitals (Fig. 5d). Meanwhile the mainly occupied orbitals at the bottom of CBs are C-2p and Pb-6p orbitals, accompanied by a small amount of Cl-3p, N-2p, Br-4p, and H-1s orbitals. The observation of the C-2p and N-2p orbitals at the top of VBs and the bottom of CBs suggests strong hybridization between C and N atoms, in other words, the delocalized π-conjugation of 4-chloro-3-methylpyridine cations. Such results indicate that the delocalized π-conjugated organic cations and the inorganic $[Pb_3Br_{10}]_n^{4n-}$ layered moieties cooperatively contribute to the optical properties of compound **2**.

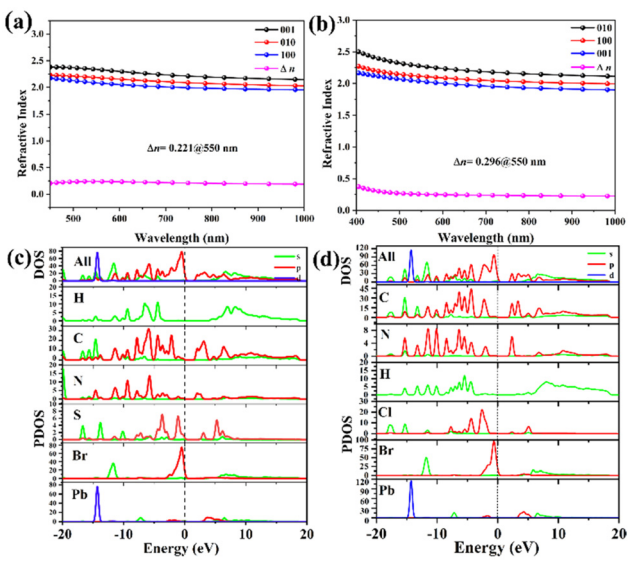

Fig. 5 The refractive index curves for (a) **1** and (b) **2**. Density of states for (c) **1** and (d) **2**.

In terms of the relationship between the structure and activity, the birefringence of the crystals is positively proportional to the structural anisotropy, which strongly depends on the structural anisotropy of the basic structural units and the space arrangement of the structural units. For elucidation of the origin of the outstanding birefringence of crystal **2**, the extent of the structural distortion of the $PbBr_6$ basic units in **1** and **2** was quantitatively evaluated using the equation[32–34]

$$\Delta d = \frac{1}{6}\sum_{n=1}^{6}[(d_n - d_0)/d_0]^2$$

where d_n and d_0 are the bond distances of the six Pb–Br bonds and the average Pb–Br bond distance, respectively. The calculated Δd value for the $PbBr_6$ octahedron is 1.4483×10^{-4} for compound **1**. In compound **2**, the Δd values for the $PbBr_6$ octahedra concerning the Pb1 and Pb2 atoms are 3.9323×10^{-4} and 1.2005×10^{-4}, respectively. Since Pb2 atom occupy an inversion center in compound **2**, the low distortion of the $PbBr_6$ octahedron regarding Pb2 is not unreasonable. As a result, the basic unit of the trinuclear $[Pb_3Br_{10}]$ unit in compound **2** containing two highly distorted $PbBr_6$ octahedra and one less distorted $PbBr_6$ octahedron exhibits larger structural anisotropy than that of the $PbBr_6$ octahedron in compound **1**. In addition, the local dipole moments for the $PbBr_6$ octahedra in **1** and **2** were calculated using a bond-valence approach.[35,36] First, the dipole moments for the six Pb–Br bonds of a $PbBr_6$ octahedron were calculated. Then a net dipole moment of a $PbBr_6$ octahedron was obtained from the vector sum of the six dipole moments of Pb–Br bonds. A net dipole moment of 3.06 Debye for the $PbBr_6$ octahedron in compound **1** is observed (Fig. S5†). The zero net dipole moment for the $PbBr_6$ octahedron regarding Pb2 in compound **2** is observed due to Pb2 possessing an inversion center symmetry, whereas a large net dipole moment of 6.85 Debye for the $PbBr_6$ octahedron regarding Pb1 in compound **2** is observed (Fig. S5†). Moreover, the directions of the dipole moments for $PbBr_6$ octahedra regarding Pb1 and Pb1A atoms are parallel to each other (Fig. S5†). Both are directed along the *b*-axis, which considerably enhances the structural anisotropy of the trinuclear $[Pb_3Br_{10}]$ basic unit in compound **2**. More importantly, the orientation of the trinuclear $[Pb_3Br_{10}]$

units in compound **2** is not antiparallelly arranged along the *b*-axis, resulting in a large vector sum of the dipole moments for a 2-D lead bromide layer in compound **2**. The 2-D lead bromide layers are parallelly packed along the *a*-axis (Fig. 2d). Thus the dipole moment of a 2-D lead bromide layer in **2** is not cancelled by the neighboring dipole moments of the 2-D lead bromide layers. Lastly, the dipole moments of organic moieties in compounds **1** and **2** were also calculated, giving a dipole moment of 1.87 Debye for di(pyridin-4-yl)sulfane cations in compound **1** and 3.27 Debye for 4-chloro-3-methylpyridine cations in compound **2**. Once again, the structural anisotropy of the organic cation of compound **2** is larger than that of compound **1**. Accordingly, the highly distorted $PbBr_6$ octahedra and the delocalized π-conjugation of 4-chloro-3-methylpyridine cations packed in an optimized arrangement mainly contribute to the large birefringence of crystal **2**.

Conclusions

In summary, two novel hybrid halide perovskites, [(H_2-dpys)($PbBr_4$)] (**1**) and [(H-cmpy)$_4$(Pb_3Br_{10})] (**2**), have been synthesized using similar reactions. [(H_2-dpys)($PbBr_4$)] (**1**) and [(H-cmpy)$_4$(Pb_3Br_{10})] (**2**) have different 2-D lead bromide layers constructed from different basic units modulated by the pyridine derivative cations. [(H-cmpy)$_4$(Pb_3Br_{10})] with trinuclear [Pb_3Br_{10}] units and delocalized π-conjugation of 4-chloro-3-methylpyridine cations exhibits large birefringence, placing it among the best birefringent crystals. The large birefringence for [(H-cmpy)$_4$(Pb_3Br_{10})] can be attributed to the highly distorted $PbBr_6$ octahedra and the delocalized π-conjugation of H-cmpy$^+$ cations in an optimal space packing as underscored by theoretical calculations. This work showcases the promising application of the halide perovskites for birefringence crystals and a feasible approach for structural and optoelectronic modulation of the hybrid halide perovskites.

Experimental

Materials and instrumentation

All chemical reagents and solvents were commercially available and used without further purification. Crystal diffraction data of **1** and **2** were collected on a Rigaku Oxford SuperNova diffractometer. The crystallographic data are presented in Table S1 (ESI†). The CIFs for **1** and **2** have been deposited in the Cambridge Crystallographic Data Centre, and the CCDC numbers are 2361167 and 2361168 for **1** and **2**, respectively.†

The birefringence of crystals **1** and **2** was obtained through a polarizing microscope (Nikon LV1000) equipped with a Berek compensator at a wavelength of 550 nm. The detailed experimental methods are provided in the ESI.†

Syntheses

Synthesis of [(H_2-dpys)($PbBr_4$)]$_n$ (1). $PbBr_2$ (110 mg, 0.3 mmol) and di(pyridin-4-yl)sulfane (47 mg, 0.3 mmol) were mixed with 4 mL of aqueous HBr solution (48% w/w). The obtained mixture was heated to 120 °C for 3 hours and transferred into a 10 mL vial, which was slowly evaporated at room temperature for 4 days. Yellow crystals were obtained (yield 64%). Elemental analysis of $C_{10}H_{10}N_2SBr_4Pb$ (717.09) (calc/found: H, 1.40/1.29; C, 16.74/15.67; N, 3.90/3.81). IR data (KBr, cm^{-1}): 1585 (s), 1465 (s), 1345 (m), 1199 (m), 1092 (m), 745 (s), 632 (w).

Synthesis of [(H-cmpy)$_4$(Pb_3Br_{10})]$_n$ (2). $PbBr_2$ (110 g, 0.3 mmol) and 4-chloro-3-methylpyridine (30 mg, 1.8 mmol) were mixed with 3 mL of aqueous HBr solution (48% w/w). The resultant mixture was heated to 100 °C for 3 hours and transferred into a 10 mL vial, which was slowly evaporated at room temperature for 3 days. Colorless crystals were obtained (yield 76%). Elemental analysis of $C_{24}H_{28}N_4Cl_4Br_{10}Pb_3$ (1934.97) (calc/found: H, 1.45/1.39; C, 14.89/14.78; N, 2.89/2.86). IR data (KBr, cm^{-1}): 1632 (s), 1592 (s), 1519 (s), 1471 (s), 1325 (m), 1252 (m), 852 (w), 698 (m), 572 (w), 525 (w).

Author contributions

Li-Ling Zhang: investigation, data curation, formal analysis, and writing – original draft. Hua Huang: methodology and writing – original draft. Qingran Ding: data curation and validation. Huiping Xiao: data curation and validation. Qing-Yan Liu: methodology, supervision, funding acquisition, and writing – review & editing. Yu-Ling Wang: conceptualization, supervision, funding acquisition, and writing – review & editing.

Data availability

The data supporting this article have been included as part of the ESI.†

Crystallographic data for compounds **1** and **2** have been deposited at the Cambridge Crystallographic Data Centre (CCDC numbers are 2361167 and 2361168 for **1** and **2**,† respectively) and can be obtained from the Cambridge Crystallographic Data Centre.

Conflicts of interest

There are no conflicts to declare.

Acknowledgements

The National Natural Science Foundation of China (22061022 and 22361021) financially supported the work. H. Huang thanks the Innovation Fund (YJS2023023).

References

1 S. Niu, G. Joe, H. Zhao, Y. Zhou, T. Orvis, H. Huyan, J. Salman, K. Mahalingam, B. Urwin, J. Wu, Y. Liu,

T. E. Tiwald, S. B. Cronin, B. M. Howe, M. Mecklenburg, R. Haiges, D. J. Singh, H. Wang, M. A. Kats and J. Ravichandran, Giant Optical Anisotropy in a Quasi-One-Dimensional Crystal, *Nat. Photonics*, 2018, **12**, 392–396.

2 M. A. Kats, P. Genevet, G. Aoust, N. Yu, R. Blanchard, F. Aieta, Z. Gaburro and F. Capasso, Giant Birefringence in Optical Antenna Arrays with Widely Tailorable Optical Anisotropy, *Proc. Natl. Acad. Sci. U. S. A.*, 2012, **109**, 12364–12368.

3 X. Chen, W. Lu, J. Tang, Y. Zhang, Y. Wang, G. D. Scholes and H. Zhong, Solution-Processed Inorganic Perovskite Crystals as Achromatic Quarter-Wave Plates, *Nat. Photonics*, 2021, **15**, 813–816.

4 A. Tudi, S. Han, Z. Yang and S. Pan, Potential Optical Functional Crystals with Large Birefringence: Recent Advances and Future Prospects, *Coord. Chem. Rev.*, 2022, **459**, 214380.

5 Z. Xie, L. Sun, G. Han and Z. Gu, Optical Switching of a Birefringent Photonic Crystal, *Adv. Mater.*, 2008, **20**, 3601–3604.

6 M. Mutailipu, K. R. Poeppelmeier and S. Pan, Borates: a Rich Source for Optical Materials, *Chem. Rev.*, 2021, **121**, 1130–1202.

7 G. Ghosh, Dispersion-Equation Coefficients for the Refractive Index and Birefringence of Calcite and Quartz Crystals, *Opt. Commun.*, 1999, **163**, 95–102.

8 H. T. Luo, T. Tkaczyk, E. L. Dereniak, K. Oka and R. Sampson, High Birefringence of the Yttrium Vanadate Crystal in the Middle Wavelength Infrared, *Opt. Lett.*, 2006, **31**, 616.

9 J. R. DeVore, Refractive Indices of Rutile and Sphalerite, *J. Opt. Soc. Am.*, 1951, **41**, 416.

10 D. E. Zelmon, D. L. Small and D. Jundt, Infrared Corrected Sellmeier Coefficients for Congruently Grown Lithium Niobate and 5 Mol.% Magnesium Oxide–Doped Lithium Niobate, *J. Opt. Soc. Am. B*, 1997, **14**, 3319.

11 Z. Guoqing, X. Jun, C. Xingda, Z. Heyu, W. Siting, X. Ke, D. Peizhen and G. Fuxi, Growth and Spectrum of a Novel Birefringent a-BaB_2O_4 Crystal, *J. Cryst. Growth*, 1998, **191**, 517–519.

12 A. Tudi, Z. Li, C. Xie, T. Baiheti, E. Tikhonov, F. Zhang, S. Pan and Z. Yang, Functional Modules Map of Unexplored Chemical Space: Guiding the Discovery of Giant Birefringent Materials, *Adv. Funct. Mater.*, 2024, 2409716.

13 M. J. Dodge, Refractive properties of magnesium fluoride, *Appl. Opt.*, 1984, **23**, 1980–1985.

14 Q. Zhang, R. An, Z. Yang, X. Long, S. Pan and Y. Yang, Review on birefringence in borates based on birefringence-active functional groups and arrangements, *Sci. China Mater.*, 2024, **67**, 2155–2170.

15 P. Gong, X. Liu, L. Kang and Z. Lin, Inorganic planar π-conjugated groups in nonlinear optical crystals: Review and outlook, *Inorg. Chem. Front.*, 2020, **7**, 839–852.

16 C. Chuangtian, W. Yebin, W. Baichang, W. Kechen, Z. Wenlun and Y. Linhua, Design and Synthesis of an Ultraviolet-Transparent Nonlinear Optical Crystal $Sr_2Be_2B_2O_7$, *Nature*, 1995, **373**, 322–324.

17 M. Zhang, D. An, C. Hu, X. Chen, Z. Yang and S. Pan, Rational Design via Synergistic Combination Leads to an Outstanding Deep-Ultraviolet Birefringent $Li_2Na_2B_2O_5$ Material with Unvalued B_2O_5 Functional Gene, *J. Am. Chem. Soc.*, 2019, **141**, 3258–3264.

18 T. T. Tran, J. He, J. M. Rondinelli and P. S. Halasyamani, $RbMgCO_3F$: A New Beryllium-Free Deep-Ultraviolet Nonlinear Optical Material, *J. Am. Chem. Soc.*, 2015, **137**, 10504–10507.

19 F. Kong, C.-L. Hu, M.-L. Liang and J.-G. Mao, $Pb_4(OH)_4(BrO_3)_3(NO_3)$: An Example of SHG Crystal in Metal Bromates Containing π-Conjugated Planar Triangle, *Inorg. Chem.*, 2016, **55**, 948–955.

20 W. Huang, X. Zhang, Y. Li, Y. Zhou, X. Chen, X. Li, F. Wu, M. Hong, J. Luo and S. Zhao, A Hybrid Halide Perovskite Birefringent Crystal, *Angew. Chem., Int. Ed.*, 2022, **61**, e202202746.

21 Q. Xu, W. Huang, H. Wang, Y. Li, Y. Zhou, L. Hou, S. Zhao and J. Luo, Designing a Dimension Reduced Hybrid Perovskite with Robust Large Birefringence by Expanding Cationic π-Delocation, *Small*, 2023, **19**, 2304333.

22 L. Liu, C.-L. Hu, Z. Bai, F. Yuan, Y. Huang, L. Zhang and Z. Lin, $2(C_3H_7N_6)^+ \cdot 2Cl^- \cdot H_2O$: An Ultraviolet Nonlinear Optical Crystal with Large Birefrigence and Strong Second-Harmonic Genertaion, *Chem. Commun.*, 2020, **56**, 14657–14660.

23 X. Dong, L. Huang, C. Hu, H. Zeng, Z. Lin, X. Wang, K. M. Ok and G. Zou, $CsSbF_2SO_4$: An Excellent Ultraviolet Nonlinear Optical Sulfate with a $KTiOPO_4$(KTP)-type Structure, *Angew. Chem., Int. Ed.*, 2019, **58**, 6528–6534.

24 Q. Jing, Z. Yang, S. Pan and D. Xue, Contribution of Lone-Pairs to Birefringence Affected by the Pb(II) Coordination Environment: A DFT Investigation, *Phys. Chem. Chem. Phys.*, 2015, **17**, 21968–21973.

25 Q. Wang, F. Yang, X. Wang, J. Zhou, J. Ju, L. Huang, D. Gao, J. Bi and G. Zou, Deep-Ultraviolet Mixed-Alkali-Metal Borates with Induced Enlarged Birefringence Derived from the Structure Rearrangement of the LiB_3O_5, *Inorg. Chem.*, 2019, **58**, 5949–5955.

26 Y. Mori, I. Kuroda, S. Nakajima, T. Sasaki and S. Nakai, New Nonlinear Optical Crystal: Cesium Lithium Borate, *Appl. Phys. Lett.*, 1995, **67**, 1818–1820.

27 A. Bauzá, T. J. Mooibroek and A. Frontera, Anhydrous Ionic Co-crystals of Cyanuric Acid with LiCl and NaCl, *CrystEngComm*, 2016, **18**, 10–23.

28 L.-L. Zhang, Q. Ding, P. Wang, Y. Zhang, Q.-Y. Liu, Y.-L. Wang and J. Luo, Achieving Strong Second Harmonic Generation Effects Induced via Dimensional Increase of PbX_6 Octahedra and Halogen Substitutes in $(C_{10}H_{11}N_3)PbX_4$ (X= Cl or Br), *Inorg. Chem. Front.*, 2024, **11**, 3618–3625.

29 T. Tong, M.-H. Lee and J. Zhang, Transformation of Optical Anisotropy Origins in Perovskite-Related Materials: A First-Principles Study, *J. Phys. Chem. C*, 2019, **123**, 31167–31174.

30 X. Zhou, X. Mao, P. Zhang, X. Dong, L. Huang, L. Cao, D. Gao and G. Zou, Designing excellent UV birefringent materials through the synergistic interaction of two highly distorted functional groups, *Inorg. Chem. Front.*, 2024, **11**, 3221–3228.

31 Q. Feng, J. Wang, C. Liu, Q. Jing and X. Dong, $NaVSeO_5$: synergistic combinations to synthesize excellent birefringent materials, *Inorg. Chem. Front.*, 2024, **11**, 3520–3526.

32 J. A. Alonso, M. J. Martínez-Lope, M. T. Casais and M. T. Fernández-Díaz, Evolution of the Jahn-Teller Distortion of MnO_6 Octahedra in $RMnO_3$ Perovskites (R = Pr, Nd, Dy, Tb, Ho, Er, Y): A Neutron Diffraction Study, *Inorg. Chem.*, 2000, **39**, 917–923.

33 J. Cheng, G. Yi, Z. Zhang, Y. Long, H. Zeng, L. Huang, G. Zou and Z. Lin, In Situ Chiral Template Approach to Synthesize Homochiral Lead Iodides for Second-Harmonic Generation, *Angew. Chem.*, 2024, **136**, e202318385.

34 L. Mao, Y. Wu, C. C. Stoumpos, M. R. Wasielewski and M. G. Kanatzidis, White-Light Emission and Structural Distortion in New Corrugated Two-Dimensional Lead Bromide Perovskites, *J. Am. Chem. Soc.*, 2017, **139**, 5210–5215.

35 I. D. Brown and D. Altermatt, Bond-Valence Parameters Obtained from a Systematic Analysis of the Inorganic Crystal Structure Database, *Acta Crystallogr., Sect. B: Struct. Sci.*, 1985, **41**, 244–247.

36 P. A. Maggard, T. S. Nault, C. L. Stern and K. R. Poeppelmeier, Alignment of Acentric $MoO_3F_3^{3-}$ Anions in a Polar Material: $(Ag_3MoO_3F_3)(Ag_3MoO_4)Cl$, *J. Solid State Chem.*, 2003, **175**, 27–33.